

DUST DIFFUSION IN LARGE-SCALE URBAN CONSTRUCTION COMBINING WRF AND CALPUFF MODEL—TAKE XIAMEN AS AN EXAMPLE

Hong ZHOU^{1*}, Binwei GAO², Fangdi DENG²

¹*School of Architecture and Civil Engineering, Xiamen University,*

Room 506, Zeng Chengkui Building, No. 182, Daxue Road, Siming District, Xiamen City, Fujian, China

²*School of Architecture and Civil Engineering, Department of Civil Engineering, Xiamen University, Fujian, China*

Received 07 January 2023; accepted 03 August 2023

Highlights

- ▶ Establishment of WRF-CALPUFF Coupling Model.
- ▶ The large-scale diffusion numerical simulation is carried out completely focus on construction dust.
- ▶ Analysis of dust diffusion law during all construction of urban construction sites working at the same time.
- ▶ Some scientific management suggestions are put forward to Xiamen city and the feasibility of the method is verified.

Abstract. With the increasing number of construction sites in cities, construction dust, as one of the essential factors affecting the atmospheric environment, urgently needs more attention. Most existing studies have studied construction dust and other particle sources comprehensively. There remains a need for research on large-scale diffusion ultimately aiming at construction dust, especially studies on the diffusion law of dust generated only by construction dust at a large-scale city level where all construction sites within the city working at the same time. To systematically explore the diffusion distribution of construction dust in such a situation, this paper takes Xiamen as the research object and puts forward a large-scale construction dust diffusion research method by integrating emission factors and combining WRF and CALPUFF model. The spatial distribution of PM₁₀ emission during the simultaneous construction of all sites in Xiamen in 2019 was simulated. The diffusion law of dust in large-scale construction in Xiamen is obtained. On this basis, the regional contribution of construction dust PM₁₀ in various districts of Xiamen and the best start month of each district are obtained, which provides valuable suggestions for government construction control. This research method can be effectively applied to cities similar to Xiamen.

Keywords: construction dust, large-scale diffusion simulation, WRF-CALPUFF combining, emission factor, construction management.

Introduction

In recent years, China has seen a number of urban construction projects. In Xiamen, for example, according to the Yearbook of Xiamen Special Economic Zone (2010–2018), the construction area in Xiamen doubled between 2010 and 2018. Research on the source of atmospheric particulate matter shows that the dust source caused by construction is one of the primary sources of urban atmospheric particulate matter (Zhang et al., 2019). The contributions of dust sources in Xiamen, Guangzhou and Nanjing to PM₁₀ were 21.7% (Song et al., 2019), 20.7% (Cui et al., 2008) and 48% (Rui et al., 2008). It can be seen

that rapid urban development not only changes the appearance of the city but also affects the environment and human health. There remains a lack of studying the diffusion law of dust generated only by large-scale city construction, urgently calling for innovative research.

A large number of construction sites in the city are under construction at the same time. According to the data provided by the Chinese Ministry of Urban and Rural Development, there were four cities in China with more than 10,000 construction sites in a single city in 2014: Tianjin, Beijing, Wuhan and Shanghai. The density of construction sites in Wuhan even reached 1.3 per square kilometer. When the construction dust generated by such a large

*Corresponding author. E-mail: mcwangzh@xmu.edu.cn

number of construction sites diffuses simultaneously, most of the particles with large particle size will directly settle down around the construction site under the action of gravity and dust control measures. However, particulates with small particle sizes such as PM_{10} and PM_{PM} will be suspended in the air for a long time and diffuse in the urban area driven by meteorological factors, resulting in atmospheric particulate pollution (Todd & Cavazos-Guerra, 2016). In addition, there are differences in construction dust emission and dust diffusion conditions at different locations of the site working at the same time. Even if the construction dust emission of a single site is lower than the allowable limit, it may eventually cause harm to the urban environment and human health. Therefore, to improve the control system of urban construction dust more effectively, it is necessary to explore the diffusion distribution of construction dust within the city.

With the continuous development of computer technology, the numerical simulation method is widely used by scholars due to its advantages of multiple factors considering capability, easy control of parameters and low price. Although the numerical simulation method is widely used, the existing research focusing only on the particle diffusion distribution from construction dust in the city is few. This is because there is considerable uncertainty in the diffusion source of construction dust, and obtaining and verifying the emission data of construction dust separately is difficult. At present, most scholars regard the construction dust source as one of the sources of urban atmospheric particulate matter and study the diffusion law of the set of particles, including construction dust in the whole atmospheric environment in the city. Gehrig and Buchmann (2003) took a long-term monitoring of PM_{10} and $PM_{2.5}$ in several Swiss cities and summarized seasonal variations of $PM_{2.5}$ and PM_{10} concentrations in different cities. CALPUFF is a three-dimensional unsteady Lagrangian diffusion model system developed by Sigma Research Corporation. Compared with the traditional diffusion model system, CALPUFF can better simulate the diffusion of pollutants over 50 km (Wu, 2018). Lee et al. (2014) used the WRF mesoscale model and the air quality model CALPUFF to simulate and verify the PM_{10} concentration distribution and contribution sources in a Yushan, South Korea park. According to the collected meteorological data and particulate emission data (Holnicki et al., 2016), simulated the diffusion process of atmospheric particulate matter PM_{10} and $PM_{2.5}$ in the Warsaw area by using the air quality model CALPUFF. Comparing the simulated concentration results with the data monitored by five air quality monitoring stations, the accuracy of CALPUFF model for global urban scale particle diffusion simulation was verified. Sówka et al. (2019) used the air quality model CALPUFF to simulate the diffusion of atmospheric particles in a Poland resort and evaluated the population's health risk based on the simulation results. Zhao (2020) established a quantitative model of heavy metal migration in the dust of 32 parks in Xiamen. Xiao et al. (2022)

studied and determined four pollution factors of $PM_{2.5}$ in Xiamen Port: industrial source, ship emission, traffic source and sea salt + construction dust mixed source.

The contribution ratio of urban building dust to the urban aerosol can vary depending on the location and time of day. In China, for instance, the human health damages caused by construction dust pollution account for 27% of the total impacts of construction projects on the natural environment (Li et al., 2020; Xing et al., 2018). Similar situations are appreciated in countries like the European Union (Maciejewska, 2008; Yassin et al., 2005). Xing et al. (2018) summarized that according to *the State of the Environment Report (2009–2012)*, PM_{10} concentrations in more than 74% of the 85 major cities are still higher than the baseline set by the Ambient Air Quality Standards, although particulate pollution in China has dropped to a lower level. For example, in Beijing, the average monthly contribution of construction dust to the overall PM_{10} pollution is about 10%. Dust emissions in some parts of Shanghai account for 12.4% of air particles. In Guiyang, it should be an eco-city in southwestern China. According to the fugitive dust measurement, this proportion is surprisingly 24.89%. In general, It has been concluded that urban building dust can contribute up to 15–30% of the total aerosol mass in urban areas, particularly during construction and demolition activities (Zhang et al., 2019). Of course, because most of the existing research focuses on a single city, there is hard to reach a unified conclusion.

Although it is challenging to analyze building dust separately, many scholars have tried and proved the value of the research on it. Aiming to map out China's practices in this area to fill the knowledge gap, Xing et al. (2018) collected and analyzed some data from 37 major cities in China for analysis and five categories of governmental measures were proposed: technological, economic, supervisory, organizational, and assessment-based. Yan et al. (2019) selected seven representative construction sites in Qingyuan city, China, for research on construction dust diffusion. In their experiment, the up-downwind method was adopted to monitor and collect TSP (total suspended particulate), PM_{10} and $PM_{2.5}$ concentrations, meteorological data and construction activities of each site, proofing that construction vehicles are one of the main influencing factors of construction dust. Chen et al. (2019) constructed the FRD $PM_{2.5}$ emissions inventory in a major inland city in China (Lanzhou) in 2017 at high-resolution ($500 \times 500 \text{ m}^2$), investigated the spatiotemporal characteristics of the FRD emissions in different urban function zones, and quantified their health impacts. Zhou et al. (2022) finished a CFD simulation of fugitive dust dispersion in a single site under different conditions during the earthwork transportation of Xiamen Metro Line 3. Inspired by the verification of studies on the set of particles that the air quality model CALPUFF and WRF mesoscale meteorological model are accurate and feasible for simulating the diffusion of particles in a large scale, Fan et al. (2020) used the air quality model CALPUFF to simulate

the diffusion of construction dust on a construction site in Chengdu. The results show that the air quality model CALPUFF can be applied to simulate the diffusion trend of construction dust on a certain scale, but it is challenging to capture the diffusion trend of construction dust on a small scale.

Admittedly, the above scholars have made an outstanding contribution to the study of the diffusion of construction dust. However, the existing studies only discuss the diffusion of dust generated by a single construction site in the city, and the scope of the study is small. There is no analysis and research focus on dust diffusion only from construction when large-scale construction sites are working at the same time in cities. There are multiple construction sites in the city working at the same time, so the research scope of construction dust diffusion at the city scale is generally more than 50 km. Considering the urgency of the research on construction dust diffusion at the city scale, this paper attempts to study the diffusion distribution of construction dust at a large scale (>50 km) based on previous valuable research. Since diffusion research based entirely on measured data is easily affected by other meteorological factors in the atmospheric environment, it is ideal for exploring the diffusion distribution law of construction dust by numerical simulation method. Referring to the existing dust diffusion research, this paper innovatively uses WRF-CALPUFF combined numerical simulation method to study the diffusion law of dust generated only by construction in a situation where all construction sites within the city working at the same time

1. Materials and methods

1.1. List establishing of emission materials

Construction dust is an open and unorganized emission source. TSP, PM₁₀ and PM_{2.5} are usually used as the analysis and monitoring indicators of construction dust diffusion.

There are many factors affecting the emission of construction dust. To quantify the emission of construction dust, the emission factor of construction dust is usually used to measure the emission of construction dust. The specific calculation formula is as follows (Song et al., 2019):

$$E = \frac{W}{S \times T}, \quad (1)$$

where E is the construction dust emission factor; W is the total emission of construction dust; S is the construction area; T is the construction time.

There are two methods to determine the emission factor. The first method is to determine the total dust emission by field measurement and then calculate the emission factor indirectly by formulae, such as the exposure height profile method (Venkatram, 2004; Veranth et al., 2003) and four-dimensional flux method (Huang et al., 2011; Song et al., 2019). Another approach is to determine according

to empirical formulas or recommended values, such as the recommended value of the *Air pollutant emission inventory compilation* (AP-42) document issued by the United States Environmental Protection Agency (1995) and the recommended values of the *Technical Guidelines for the Compilation of Dust Source Particle Emission Inventory (Trial)* document in China (Ministry of Ecology and Environment the People's Republic of China, 2014). This study aims to investigate the diffusion patterns of dust generated solely from building construction sites that are simultaneously active in large cities, considering the vast number and wide distribution of construction dust sources. As such, assigning weights to each individual basis of construction dust may result in an enormous computational workload and difficulty obtaining accurate data and parameters, potentially affecting the feasibility and accuracy of the study. In addition, in the existing urban-scale diffusion simulation studies in China, scholars mostly use the first overall estimation method (Fan et al., 2022; Yang et al., 2022; Yang, 2014; Zhang et al., 2019). Among them (Yang et al., 2022), pointed out that the contribution rate of construction dust to urban atmospheric PM₁₀ can be close to 20%, and its environmental impact has an increasing trend year by year. The contributions of dust sources in Xiamen, Guangzhou and Nanjing to PM₁₀ were 21.7%, 20.7%, and 48% (Song et al., 2019). Therefore, the method of overall estimation is adopted in this study, referring to the primary calculation parameter of existing research conclusions on the composition of construction dust in Xiamen.

Technical Guidelines for the Compilation of Dust Source Particle Emission Inventory (Trial) issued by the Ministry of Environment provides a series of emission factors applicable to the Chinese environment based on domestic monitoring and experimental data after being field validated and evaluated. The US Environmental Protection Agency (EPA) AP42 database is a set of emission factors mainly developed by the US EPA based on monitoring and experimental data mainly from the US and Canada regions. However, the differences between the Chinese recommended values and the US EPA AP42 data may be related to different monitoring and experimental methods. In China, the compilation of particulate matter emission inventories is usually carried out by provincial environmental protection agencies, which adopt standardized monitoring and practical strategies according to national standards and guidelines. Different monitoring and experimental methods may be adopted in the US and Canada, resulting in differences in data. Furthermore, this guideline was issued several years after the publication of the US EPA AP42, which is an internationally recognized foundation standard and one of the reference standards for this guideline. The Ministry of Ecology and Environment has openly explained that this guideline fully consolidates and summarizes the research results of major research institutions, which can be used to guide environmental protection departments at all levels to carry out the

PM₁₀ emission inventory preparation work scientifically and normatively, obtain PM₁₀ emission inventory results based on uniform methodology and data sources, and provide scientific and effective support for the formulation of particulate matter pollution control strategies. Since our case study is based on a Chinese urban scenario, adopting the recommended values from the Chinese 2014 Technical Guidelines for Preparation of Dust Source Particulate Matter Emission Inventory (Trial) is more appropriate and consistent with the actual situation in China. Therefore, considering the previous methods for determining the construction dust emission factors, this paper adopted the construction dust emission factors recommended by the *Technical Guidelines for the Compilation of Dust Source Particle Emission Inventory (Trial)* issued by the Ministry of Environment in 2014 and used them to construct the construction dust emission list of Xiamen in 2019. The formula is as follows:

$$E_Z = 2.69 \times 10^{-4} \times (1 - \eta), \tag{2}$$

where E_Z is the emission factor of construction dust TSP (Total suspended particles in the air) under the overall estimation; η represents the dust removal efficiency as shown in Table 1.

Table 1. Value of η under different dust suppression measures (Ministry of Ecology and Environment the People's Republic of China, 2014)

Dust suppression measures		η (%)		
		TSP	PM ₁₀	PM _{2.5}
Pavement paving and Water spraying	Paving concrete, sprinkling strength	96	80	67
	Dust screen			
	Nylon plastic mesh diameter 0.5 mm, mesh distance 3 mm	24	20	17
	Nylon plastic mesh diameter 1 mm, mesh distance 5 mm	12	10	8
Cover dustproof cloth	High strength fiber fabric closed cover	32	27	22
	Nylon plastic mesh diameter 1 mm, mesh distance 5 mm	20	17	14
Chemical dust suppressor		89	84	71
Enclosure	2.4 m hard enclosure	18	15	13
	1.8 m hard enclosure	12	10	8

According to the data provided by Xiamen Construction Bureau, the number of all key construction sites in Xiamen in 2019 was counted (Statistics, 2020) (the types of construction sites including municipal road projects, building demolition projects and general construction projects) and smaller construction sites was eliminated. Then the geographical location information (latitude and

longitude) of each site, the construction area of the site, the number of active months in the year, and the dust suppression measures were investigated to obtain the basic parameters. Finally, the emission factor method is used to calculate the construction dust emission (PM₁₀) of all key construction sites in the list, and the construction dust emission list of all construction sites in Xiamen in 2019 is obtained, as shown in Table 2.

Table 2. Site information and construction dust emission list in Xiamen in 2019

District	Number of construction sites	Construction area (Hectare)	Dust emissions(t)		
			PM _{2.5}	PM ₁₀	TSP
Siming	26	91.75	1938	8600	15 316
Huli	49	137.03			
Xiang'an	72	239.41			
Haicang	24	91.35			
Jimei	34	141.32			
Tong'an	32	165.67			

As can be seen from Table 2, PM₁₀ emissions are about 4.5 times higher than PM_{2.5}. The TSP includes PM₁₀ and PM_{2.5}. Existing research also shows that dust emissions PM₁₀ is more enormous than PM_{2.5}. Most of those studies use PM₁₀ as the primary monitoring indicator for dust research (Qin et al., 2020; Yang et al., 2022). Zhu (2020) pointed out that meteorological conditions have a more significant impact on urban PM_{2.5} concentration, and less effect on PM₁₀. Because this paper focuses on simulating the large-scale diffusion of construction dust in the metropolitan area of Xiamen in the case of all construction sites working at the same time, the influence of meteorological conditions should be avoided as much as possible. Moreover, it is more matchable and appropriate to select a specific dust factor with a more significant proportion of dust emission rather than a factor representing the total suspended particles in the air for simulation on the larger scale of the simulation. Besides, research has proved that over 85% of 74 major cities still have a PM₁₀ concentration higher than the baseline specified in the Ambient Air Quality Standard (Xing et al., 2018). Therefore, PM₁₀ is of good typicality and used as the focused index of construction dust in this paper for the above reasons.

1.2. Simulation methods

As shown in Figure 1, Xiamen is located on the southeast coast of Fujian Province, China, with a latitude of 24.418–24.903 in the north and 117.866–118.415 in the east. The administrative division of Xiamen can be divided into Siming District, Huli District, Xiang'an District, Haicang District, Jimei District, and Tong'an District. The land area is 1699.39 square kilometers, and the sea area is more than 300 square kilometers. The overall terrain of Xiamen is high in the northwest and low in the southeast. The highest altitude of the city is 1175.2 meters. From northwest

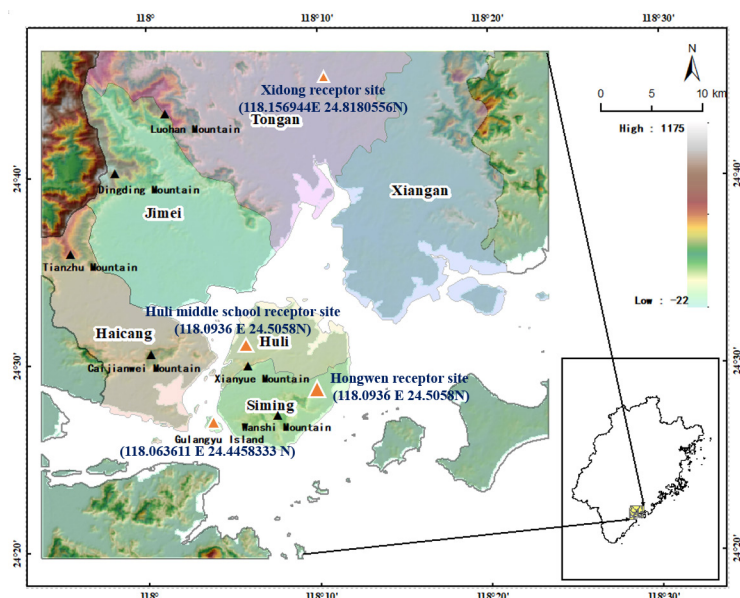


Figure 1. Overall situation of Xiamen City and four discrete receptor sites

to east, the topography and terrain are distributed in high mountains, low hills, terraces, plains and beaches.

According to the 2018 National Economic and Social Development Statistics Bulletin issued by the Xiamen Municipal Bureau of Statistics, the annual gross regional product (GDP) is 479,141 million yuan, an increase of 7.7%. The data show that in recent years, the value added of all construction industries in Xiamen has shown an upward trend. The research on it can not only provide a theoretical basis for the construction management and control of Xiamen, but also provide a reference for cities similar to Xiamen, thus providing a research basis for the future study of large-scale urban dust.

In order to evaluate the accuracy and reliability of the numerical simulation results, the method of comparing and verifying the monitoring values and simulation values was adopted in this study. The monitoring data were collected from four national air quality monitoring stations in Xiamen City (Gulangyu, Huli middle school, Hongwen, and Xidong). Therefore, four discrete receptor points were set up in this study, and the coordinates of the four discrete receptor points were consistent with those of the four national air quality monitoring stations in Xiamen City. The specific locations and coordinates are shown by the orange triangle in Figure 1.

1.2.1. CALPUFF and WRF

Currently, the mainstream environmental quality regulatory models include the AERMOD and CALPUFF models recommended by the U.S. Environmental Protection Agency (EPA). These two models are also recommended models in the “Technical Guidelines for Environmental Impact Assessment - Atmospheric Environment” (HJ 2.2-2018) published by the Ministry of Ecology and Environment of China (2018). Studies have shown that the CALPUFF model, a Lagrangian-Gaussian plume model, has

higher computational accuracy and is more suitable for large-scale spatial pollution impact analysis and prediction (greater than 50 km). In comparison, AERMOD is a steady-state plume model that is more suitable for pollution impact analysis and forecast in medium to small spatial ranges (less than 50 km) (Li et al., 2020; Xu et al., 2022; Zhang et al., 2022; Zhao & Li, 2018). Additionally, the CALPUFF model considers various factors, such as complex terrain and meteorological parameters, which results in more reasonable simulation results for sudden changes in wind direction and improved handling of calm wind conditions compared to the AERMOD model. In addition, the CALPUFF model integrates various aspects, such as complex terrain, meteorological parameters, etc., and produces simulation results that are more reasonable than those of the AERMOD model, particularly in simulating wind direction changes and handling calm wind conditions (Li et al., 2020). Moreover, based on a study of a coastal oil refinery in the United States (Fisher et al., 2003), found that traditional Gaussian plume dispersion models struggle to accurately simulate the dispersion of pollution from coastal sources. However, with sufficient meteorological data, the use of the non-steady-state Lagrangian particle model CALPUFF provided simulation results for pollutant concentrations that were closest to actual measurements. In the study of flue gas diffusion simulation in coastal power plants (Zhao et al., 2015), also recommended the application of Calpuff model in the simulation of coastal diffusion. Xiamen is a coastal city in southeastern China, with a complex terrain of mountains, hills, and plains. The city has a subtropical monsoon climate, with significant seasonal and daily temperature variations and abundant rainfall. The sea-land breeze circulation, mountain-valley breeze circulation, and the passage of typhoons influence the local wind patterns. All these factors can somewhat affect the dispersion and

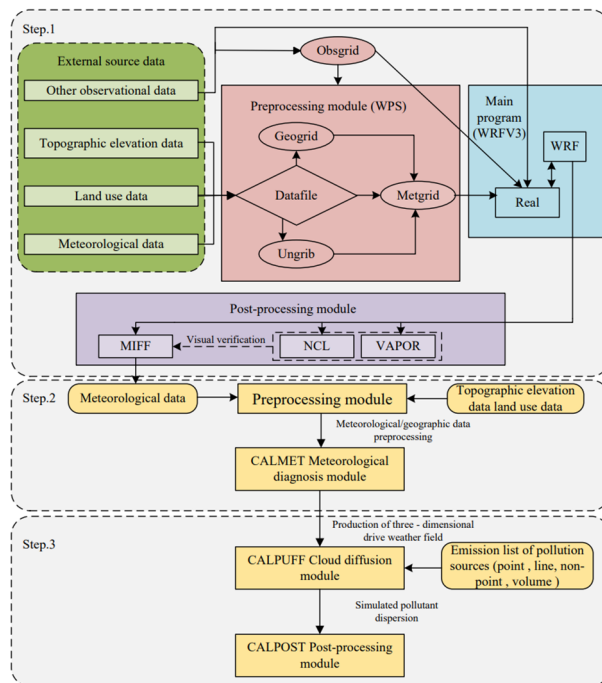


Figure 2. Farmwork of the combination of the WRF and CALPUFF model

transportation of dust in the city. Therefore, CALPUFF, which shows a more reasonable result for the above factors, is chosen in this paper.

The data that CALPUFF model system needs to input include meteorological data (Ground meteorological data and High altitude meteorological data), topographic elevation data, land use data and pollutant emission inventory data. Compared with the ground meteorological data, the detailed and accurate high altitude meteorological data are challenging to obtain. Therefore, this paper attempts to integrate WRF and CALPUFF model. The combination of ground observation meteorological data and advanced meteorological simulation data from WRF mesoscale meteorological model was realized and finally was used by CALPUFF model to simulate the diffusion distribution of long-distance pollutants over 50 km of construction dust PM_{10} monitoring index. The farmwork of the combination model is illustrated in Figure 2.

The combining of CALPUFF and WRF is mainly achieved through the integration of CALMET and WRF to provide high-altitude meteorological data, which improves the simulation accuracy of CALPUFF. CALMET is the meteorological preprocessing program for CALPUFF, which provides the high-altitude meteorological data required by CALPUFF. WRF can provide meteorological data in both horizontal and vertical directions, playing an essential role in delivering high-resolution meteorological forecast data to more accurately reflect atmospheric motion and radiation transmission processes (Guo et al., 2020).

The Weather Research and Forecasting (WRF) is the latest-generation mesoscale numerical weather prediction model and was developed by the National Center for

Atmospheric Research (NCAR), the Pacific Northwest National Laboratory (PNNL) and the National Oceanic and Atmospheric Administration (NOAA) (Peckham, 2012). The WRF mesoscale meteorological model is usually used in the field of atmospheric science to predict meteorological conditions on a large scale, and it can also be used as a pollutant-driving field in the field of air quality model and computational fluid dynamics (Akhmetshina et al., 2015). WRF has two versions: ARW (Advanced Research WRF), developed from the MM5 model and NMM (Nonhydrostatic Mesoscale Model) developed from the Eta model. The former is mainly used for research and application, while the latter is for business use. ARW is used for meteorological forecasts in this paper.

WRF model consists of three main components: the preprocessing module (WPS), the main program module (WRFV3), and the post-processing module (Skamarock et al., 2008). The workflow of the model is illustrated in step 1 in Figure 2.

The WPS includes three subprogram modules, Geogrid, Ungrid, and Metgrid. Geogrid defines the simulation area, determines the number of grid nesting levels, grid size, and the number of vertical layers, and interpolates terrain elevation data and land use data into the simulation area grid. Ungrid extracts meteorological field data saved in Grib format. Metgrid interpolates the extracted meteorological field data into the simulation area grid. The main program module (WRFV3) consists of two parts, the real program and the WRF program. The real program processes the output files from the WPS module. The WRF sector uses the Advanced Research WRF (ARW) to solve the fully compressible non-hydrostatic balance equations with the balance option. The post-processing module extracts the results of WRF output. To accurately describe the physical processes at the grid scale, NCL (NCAR Command Language) and VAPOR (Visualization and Analysis Platform for Ocean, Atmosphere, and Solar Researchers) are used to visualize the physical processes and assist in determining the feasibility of processing data. MIFF is used to extract the parameters of the CALPUFF dispersion module output by the WRF forecast meteorological model and the direct input format (Choi et al., 2018; Lim et al., 2021).

The CALPUFF model system comprises four sub-modules: the preprocessing module, meteorological diagnostic module, dispersion module, and post-processing module. The core of the preprocessing module is the CALMET program, which links WRF and CALPUFF, as shown in step 2 in Figure 2. This module converts observed meteorological data and high-altitude meteorological data simulated by the WRF mesoscale meteorological model after MIFF transforming into a format that the CALMET meteorological diagnostic module can recognize. It extracts ground characteristic parameters, such as roughness, albedo, and Bowen ratio, required by the CALMET module and generates files in a format recognizable by the CALPUFF dispersion module. Subsequently, a three-dimensional meteorological field is provided for the CALPUFF diffusion

module to generate the meteorological element data that can be identified by the CALPUFF diffusion module (Lei et al., 2021; Lim et al., 2021).

The CALPUFF diffusion module, as shown in step 3 in Figure 2, reads the three-dimensional meteorological field file output by the CALMET meteorological diagnostic module and uses it as the driving condition, combined with emission inventory information of point sources, line sources, area sources, volume sources, and other information, to simulate the transportation and transformation processes. CALUPFF module has two sets of concentration equations, the basic concentration equation and the Slug equation. The Slug equation is applicable to local-scale pollution problems.

The fundamental concentration equation is as follows (Li & Guo, 2006):

$$C = \frac{Q}{2\pi\sigma_x\sigma_y} g \times e^{\frac{-d_a^2}{2\sigma_x^2}} \times e^{\frac{-d_c^2}{2\sigma_y^2}}; \quad (3)$$

$$g = \frac{2}{\sigma_z\sqrt{2\pi}} \sum_{n=-\infty}^{\infty} e^{\frac{-(H_e+2nh)^2}{2\sigma_z^2}}, \quad (4)$$

where C is the mass concentration of ground pollutants at any grid point; Q is the source strength; σ_x is the diffusion coefficient of X direction; σ_y is the diffusion coefficient of Y direction; σ_z is the diffusion coefficient of Z direction; d_a is the downwind distance; d_c is transverse distance; H_e is the effective height; h is the height of the mixing layer; g is the vertical term of the Gauss equation.

Slug equation is as follows (Bo et al., 2009):

$$C = \frac{F \times Q}{\sqrt{2\pi} u' \sigma_y} g \times e^{\frac{-d_a^2 u^2}{2\sigma_y^2 u'^2}}; \quad (5)$$

$$F = \frac{1}{2} \left\{ \operatorname{erf} \left(\frac{d_{a2}}{\sqrt{2\sigma_{y2}}} \right) - \operatorname{erf} \left(\frac{-d_{a1}}{\sqrt{2\sigma_{y1}}} \right) \right\}, \quad (6)$$

where Q is the source strength; u is the average wind vector; u' is the average wind speed (scalar); F is the causal function; erf is the error function.

Finally, the CALPOST post-processing module is used to extract the meteorological element data of the meteorological module and the concentration data and dry and wet deposition data in the diffusion module, and the extracted data are presented in the form of graphic visualization (Xu et al., 2019).

1.2.2. Meteorological simulation

The initial meteorological data should be input before using CALPUFF model to simulate the dust diffusion in urban construction, and then CALMET module was used to output the hourly background meteorological field as the driving condition of dust diffusion in construction. The initial meteorological data include ground meteorological

monitoring data and high-altitude meteorological data. In this paper, the high-altitude simulated meteorological data were obtained through the WRF mesoscale meteorological model simulation. The initial field and boundary conditions were based on the global reanalysis data of $1^\circ \times 1^\circ$ FNL format provided by NCEP (National Center for Atmospheric Research, USA). The topographic elevation data were based on the SRTM90 data of USGS. The land use data were based on MODIS satellite data. Ground meteorological data was from hourly monitoring data of ground monitoring meteorological station Xiamen station. The number of Xiamen station site was 59134, 118.07 E, 24.48 N, site elevation 140.6 m.

The WRF mesoscale meteorological model, CALMET module and CALPUFF module are all involved in the simulation range setting and grid division, and the relationship between the three is inclusive. The mesoscale double-layer grid nested WRF meteorological model was adopted. The grid center was located in the center of Xiamen Island. The coordinates of the center were 118.281 E and 24.407 N. The simulation range of outer layer d01 was 1350×1350 km, and the grid resolution was 13.5 km. The simulation range of inner layer d02 was 450×450 km, and the grid resolution was 4.5 km. The innermost layer d03 was the simulation range of CALMET module and CALPUFF module, which included the whole city of Xiamen. The coordinates of the center point were 118.14E and 24.33N. The grid resolution was 500 m, totaling 100×100 grids. In the vertical direction, the WRF mesoscale meteorological model was set to 38 layers, and the top-level pressure of the model was set to 50 hPa. From bottom to top, the model was linearly stratified according to the pressure. CALMET module and CALPUFF module had 8 layers in the vertical direction, which were 20 m, 50 m, 200 m, 500 m, 1500 m, 2200 m, 3300 m and 4000 m respectively. The WRF, CALPUFF, CALEMET Horizontal Simulation Grid Range was shown in Figure 3a.

The simulation time ranges of WRF mesoscale model, CALMET module and CALPUFF module were set from 00:00 on January 01, 2019 to 00:00 on January 01, 2020, with a total of 8760 hours. The remaining parameters used the default recommended values from U.S. Environmental Protection Agency (EPA) (Bo et al., 2009).

Four kinds of pollution source data can be input into CALPUFF module, including point source, line source, surface source and bulk source. The parameters required for different pollution sources are different. The accuracy of CALPUFF module simulation results depends on the value of relevant parameters of pollution sources (Li, 2014). According to the actual situation, the pollution sources were divided according to the construction site type. This paper divided municipal road engineering into line sources, and general construction engineering, demolition engineering, and other site types were divided into non-point sources. Without considering the point source and body source, 182 non-point sources and 55 line sources were finally determined, as shown in Figure 3b.

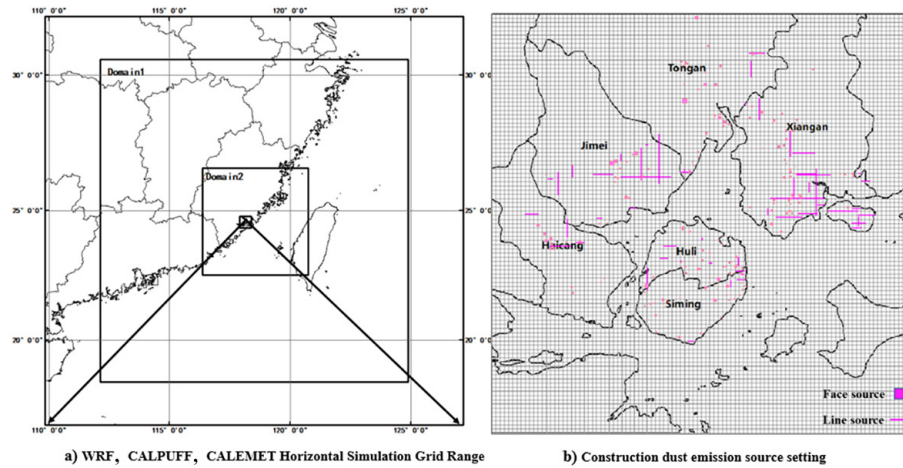


Figure 3. Horizontal Simulation Grid Range and Construction dust emission source setting

2. Results and discussion

2.1. Overall and credibility analysis

To evaluate the numerical simulation results' accuracy and reliability, the monitoring and simulation values were compared and verified in this paper. The monitoring data were from the daily average PM_{10} concentration data of the whole year in 2019 collected by Xiamen National Air Quality Monitoring Station (Gulangyu, Huli Middle School, Hongwen and Xidong). Although Calpuff allows assessing hourly values, by referring to the research of other scholars, we finally did not choose to simulate hourly data for dust diffusion in large-scale urban models for its inaccuracy in hourly simulation. For instance (Holnicki et al., 2016), used the CALPUFF model to simulate concentrations of PM_{10} , $PM_{2.5}$, CO, and benzene (C_6H_6) in the Warsaw metropolitan area. The results indicated that the model performed well in predicting annual average values but had poor time-consistency accuracy in short-term (1-hour average) concentrations, particularly under low wind meteorological conditions. These findings support the limitations of the CARPUFF model for short-term forecasting in complex near-field environments, as proposed by (Cui et al., 2011). Guo et al. (2020), Tartakovsky et al. (2016) also supported these conclusions in their papers. Therefore, we believe that considering hourly emission data may not necessarily improve the accuracy of dust diffusion simulation in large-scale urban models, and further research is needed to explore this issue.

It should be noted that the contribution sources of PM_{10} concentration monitored by air quality monitoring stations include vehicle sources, industrial sources and other sources in addition to construction dust sources. Research showed that the proportion of dust sources in Xiamen is about 21.7% (Song et al., 2019). Objectively, because the data monitored by the air pollutant monitoring station are the data of PM_{10} in the whole atmosphere, it is pretty hard or nearly impossible to obtain the PM_{10} generated only by the construction dust diffusion separately, which undoubtedly brings some challenges

to the comparison of the results. Therefore, the observation results are adopted to match this problem in this paper. Based on the assumption that the constant 21.7% contribution of construction to measured concentrations everywhere in the town, it is necessary to preprocess the original monitoring data before comparative verification, which should be multiplied by 21.7%.

The calculation of 5 statistical analysis indexes of 4 discrete receptor points was based on Equations (7)–(11) (Liu, 2015; Yang et al., 2019; Zhang et al., 2006; Zhang et al., 2013a, 2013b).

$$\bar{C}_{Sim} = \frac{1}{N} \sum_{i=1}^N C_{Sim_i}; \tag{7}$$

$$\bar{C}_{Obs} = \frac{1}{N} \sum_{i=1}^N C_{Obs_i}; \tag{8}$$

$$r = \frac{\sum_{i=1}^N (C_{Sim_i} - \bar{C}_{Sim})(C_{Obs_i} - \bar{C}_{Obs})}{\sqrt{\sum_{i=1}^N (C_{Sim_i} - \bar{C}_{Sim})^2} \sqrt{\sum_{i=1}^N (C_{Obs_i} - \bar{C}_{Obs})^2}}; \tag{9}$$

$$NMB = \frac{\sum_{i=1}^N (C_{Sim_i} - C_{Obs_i})}{\sum_{i=1}^N C_{Obs_i}}; \tag{10}$$

$$NME = \frac{\sum_{i=1}^N |C_{Sim_i} - C_{Obs_i}|}{\sum_{i=1}^N C_{Obs_i}}; \tag{11}$$

where C_{sim_i} and C_{Obs_i} are the i th simulation value and i th monitoring value respectively, $N = 365$. The correlation coefficient r reflects the correlation between the monitoring value and the simulation value. The closer r is to 1, the higher the correlation between the monitoring value and the simulation value is, and the better the simulation effect is. NMB and NME belong to dimensionless statistics. NME reflects the average deviation between monitoring value and simulation value, and NMB reflects the average

absolute error between monitoring value and simulation value. The smaller the error is, the better the simulation effect is (Wu, 2018).

The calculation results are shown in Table 3. The correlation coefficients r of the four discrete receptor points were above 0.8, indicating that the correlation between the simulation results and the real monitoring values was strong, and the simulation results were good. The NMB of four national control sites were negative ($-18.5\% \sim -26.4\%$), indicating that the simulation value was generally less than the monitoring value, but the deviation was in a reasonable range. The sources of analysis errors were as follows: 1) There were certain errors in the statistics of the emission inventory itself so that the emission may be underestimated; 2) The PM_{10} concentration extracted from the discrete receptor point was the average value in a grid while the concentration data monitored by the national control point were the concentrations at a specific point; 3) To eliminate the influence of other pollution sources on the PM_{10} monitoring data of the air monitoring station, this paper used a proportional coefficient to reduce the monitoring value, which was a reference value obtained through the source analysis experiment.

To further compare the error relationship between the simulation value and the monitoring value, the daily concentration time series change diagram and the monthly

Table 3. PM_{10} Statistical analysis results of monitoring and simulation values

AQMS	\bar{C}_{Sim} , ug/m ³	\bar{C}_{Obs} , ug/m ³	r	NMB	NME
GLY	6.69	8.19	0.84	-18.5%	49.2%
HLMS	6.46	9.75	0.91	-33.8%	39.1%
HW	6.35	8.06	0.91	-21.2%	34.0%
XD	6.08	7.91	0.91	-26.4%	32.4%

concentration time series change diagram of the simulation value and the monitoring value of the four discrete receptor points were drawn, as shown in Figure 4 and Figure 5.

Overall, the monthly concentration variation trends of the simulated and monitored values of the four discrete receptor points were not significantly different. In addition to Gulangyu, the daily concentration variation trends of the monitored values and simulated values of the three discrete receptor points were also basically consistent. Reasons: Gulangyu is a small island surrounded by the ocean. The grid resolution set in the CALPUFF module was 500 m. Affected by the terrain resolution, this block's short-term concentration simulation value may be distorted. The best simulation time was the second half of

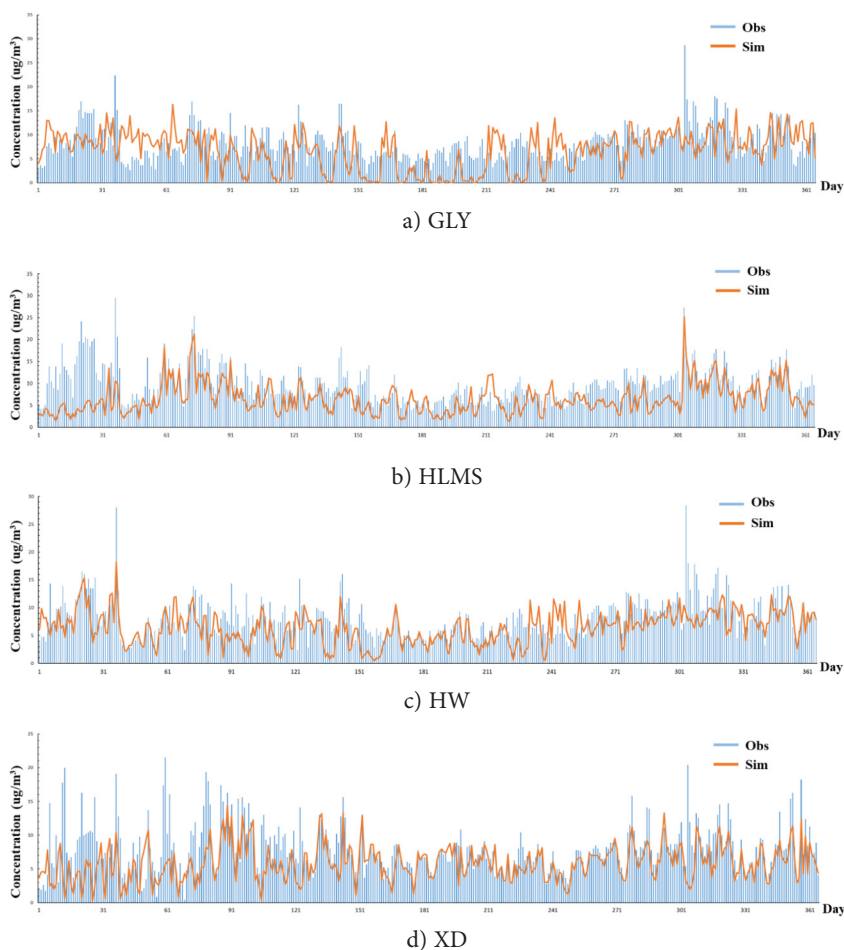


Figure 4. Time series diagram of daily concentration of discrete receptor monitoring values and simulated values

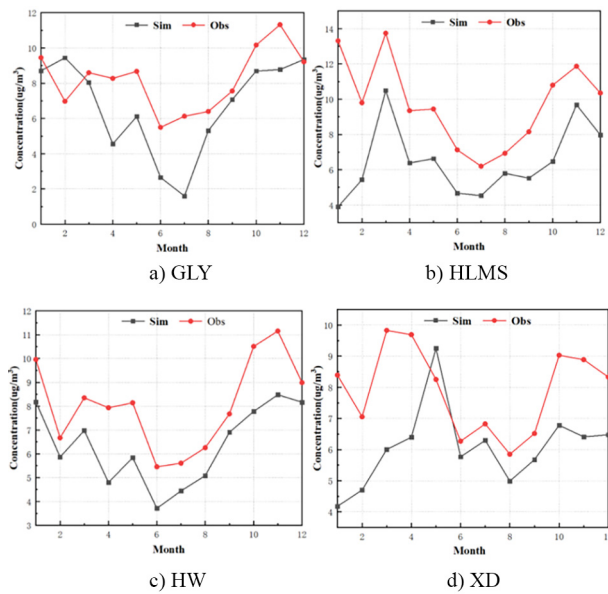


Figure 5. Monthly concentration time series of monitored and simulated values at discrete receptor points

the year. The monthly concentration and daily concentration errors of simulated values were mainly from the first three months.

To eliminate the interference of other sources on the monitoring value of PM_{10} concentration, the method used in this paper was to reduce the monitoring value through a unified proportional coefficient. Therefore, the error here may be from the reduced monitoring value. However, because CALPUFF is suitable for simulating long-term concentration, this paper chooses to simulate one-year construction dust diffusion. In the long run, the error between the simulation results and the observed results is within an acceptable range, and the model’s simulation results meet the requirements to a certain extent.

2.2. Spatial distribution of construction dust emission

According to the emission list, the construction dust emissions were counted. The statistical results are shown in Table 4. Results show that there were 237 large and small construction sites in Xiamen in 2019. Among the six districts of Xiamen City, Xiang’an District had the most significant number of construction sites, the largest construction area, and the largest PM_{10} emission. Haicang District had the least number of construction sites and the smallest construction area. Siming District had the minimum PM_{10} emissions.

Table 4. Statistics of dust emission from key construction sites in Xiamen in 2019

District	Siming	Huli	Xiang’an	Tong’an	Jimei	Haicang
Number of construction sites	26	49	72	32	34	24
construction area (million square)	91.75	137.03	239.41	165.67	141.32	91.35
PM_{10} discharge amount (t)	646.9	1443.3	2910.7	1734.4	1175.0	689.6

Figure 6 shows the spatial distribution map of PM_{10} emission in construction sites considering dust suppression measures. It can be seen that the construction sites outside the center island were mainly distributed in the south of Xiang’an District, the junction of Tong’an District and Xiang’an District, the middle of Jimei District and the northwest of Haicang District. There were large dust emission sites in the four areas outside the center island. Large dust emission sites in Xiang’an District were gathered in the south; the distribution of large dust emission sites in Tong’an District; large dust emission sites in Jimei District were primarily concentrated in the middle; large dust emission sites in Haicang District were gathered in the northwest.

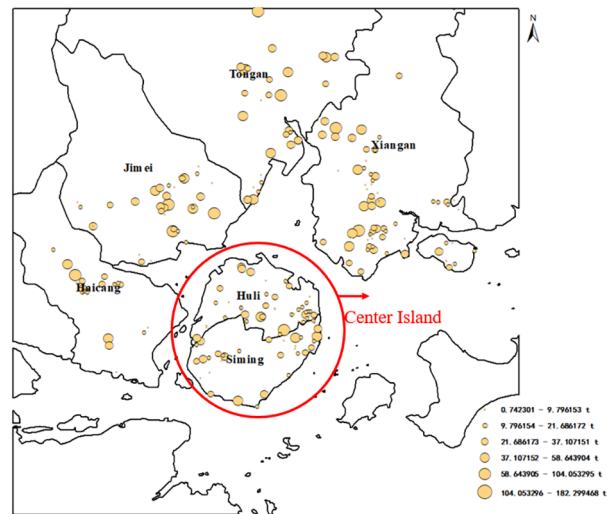


Figure 6. Spatial emission distribution of construction dust PM_{10}

2.3. Analysis of simulated diffusion results of annual average concentration

Figure 7 shows the average annual concentration diffusion cloud map of PM_{10} in Xiamen 2019 construction dust. It can be seen that in 2019, the overall diffusion range of construction dust PM_{10} in Xiamen City was from northeast to southwest, and the diffusion range was more than 1402 km^2 , accounting for 56.1% of the simulation range. The average annual concentration range of PM_{10} in construction dust was 0–132.5 ug/m^3 . Areas whose diffusion range ($>70 ug/m^3$) exceeded the concentration limit of the second class were mainly concentrated in the southern junction of Tong’an District, Xiang’an District, the middle of Tong’an District, the west and east of the center island, the northwest of Haicang District and the south of

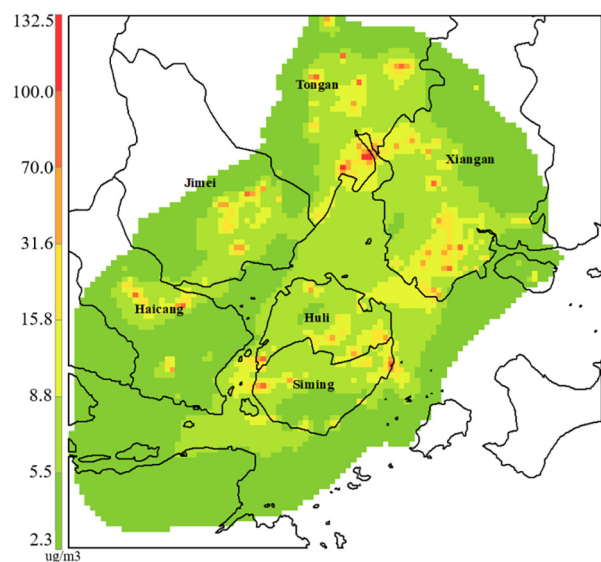


Figure 7. Map of annual concentration diffusion of construction dust PM_{10}

Xiang'an District. Among them, the average annual concentration of construction dust PM_{10} in Tongan District and the southern border of Xiang'an District was the highest in Xiamen City.

To further study the formation mechanism of annual concentration diffusion results in Xiamen, the PM_{10} diffusion of construction dust under separate construction in Xiamen was simulated. Figure 8 shows the concentration diffusion map and annual wind field map of construction dust PM_{10} under separate construction in each district.

The results show that PM_{10} diffused around the high-concentration area as the core, offering a spot-like diffusion trend as a whole. PM_{10} generated from the construction site in Siming District is concentrated in the east, west and south of Siming District. Construction dust PM_{10} is focused on the east and west of Siming District, with the highest annual concentration of 132 ug/m^3 . Because the dominant wind direction is north wind and northwest

wind, construction dust PM_{10} mainly diffuses south and southwest, and the general diffusion area is 60.25 km^2 .

The diffusion range of PM_{10} produced by the Huli District construction site covers the entire Huli District, the northern part of Siming District and the western sea area of Xiamen Island. The maximum annual concentration of dust PM_{10} during construction is 101.5 ug/m^3 . The annual dominant wind direction in Huli District is north wind so that the construction dust PM_{10} mainly spreads southward. Due to the obstruction of Wanshi Mountain in the middle of Siming District, the construction dust PM_{10} can only be transported to the northern and southwestern sea areas of Siming District. The overall diffusion range of construction dust PM_{10} is 126.5 km^2 .

The diffusion range of PM_{10} produced by the construction site in Xiang'an District is a zonal distribution from northeast to southwest. The diffusion range covers most areas in the southwest of Xiang'an District, southwest sea area, east of Huli District, and east of Siming District. The number of construction sites in Xiang'an District is the largest, and the distribution is relatively dense, mainly concentrated in the south-central and northwest of Xiang'an District, and the high concentration area is also primarily concentrated in these two areas. However, the highest annual concentration is less than 100 ug/m^3 , which is the lowest in the six districts of Xiamen. Combined with the analysis of reasons in Figure 1, the building density in Xiang'an District is low. There is no tall building block. The terrain is flat and the wind is relatively strong. The diffusion conditions of construction dust PM_{10} are the best. The annual dominant wind directions in Xiang'an District are northeast wind and north wind. Therefore, the construction dust PM_{10} spreads to the southwest under the action of the prevailing wind direction. The diffusion range (330.25 km^2) is the largest in the six districts of Xiamen.

The diffusion range of PM_{10} produced by the construction site in Tong'an District shows a strip distribution from north to south, covering the eastern half of

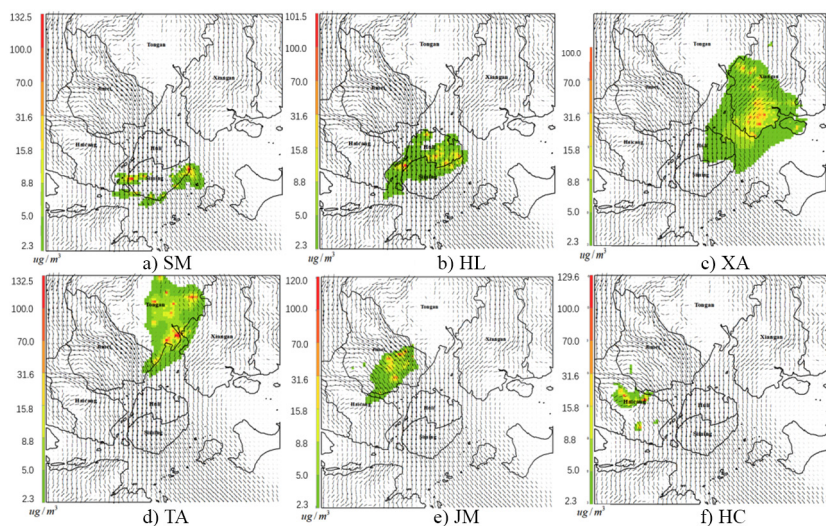


Figure 8. Annual concentration diffusion map and annual wind field map of construction dust PM_{10} in each district of Xiamen

Tong'an District, the western part of Xiang'an District and the southern sea area of Tong'an District. The high concentration area of construction dust PM_{10} is concentrated in the southeast and central of Tong'an District. The PM_{10} emission of construction dust in Tong'an District is the second in the city, but due to the low wind speed in Tong'an District, the average annual concentration of PM_{10} in construction dust in Tong'an District is the highest at $132.5 \mu\text{g}/\text{m}^3$.

The diffusion range of PM_{10} generated by the start of construction in Jimei District is zonally distributed from northeast to southwest, covering the southeast of Jimei District and the north of Haicang District. The high concentration area of construction dust PM_{10} is concentrated in the central part of Jimei District, and the highest annual average concentration is $120.0 \mu\text{g}/\text{m}^3$. The annual dominant wind direction in Jimei District is northwest wind. It is blocked by dense buildings in the south of Jimei District in the process of diffusion and transfer of construction dust PM_{10} . The lateral diffusion is apparent. The construction dust PM_{10} spreads to the southwest and northeast, and the overall diffusion range is 74.25 km^2 .

PM_{10} produced by Haicang construction site is concentrated in the northwest and south of Haicang. The high concentration area of construction dust PM_{10} is focused on the northwest of Maluan Bay in Haicang District, with the highest average annual concentration of $129.6 \mu\text{g}/\text{m}^3$, after Tong'an District. Combined with Figure 1, with a large number of construction sites in this region, the blocking of Caijianwei Mountain in the south and a rotational wind here, the construction dust PM_{10} converges here. It cannot be diffused and transferred to a farther place. Finally, the construction dust PM_{10} concentration

in this region is high, and the overall diffusion range which is only 30.5 km^2 of Xiamen is the smallest in the six districts.

2.4. Analysis of simulated results of concentration of representative month

For the subtropical climate in Xiamen, autumn and winter last for a short time, usually only one month. Therefore, to study the diffusion law of PM_{10} of construction dust in Xiamen city in different seasons, this paper used the representative months to represent different seasons. The representative months of winter, spring, summer and autumn were January, April, July and November. Figure 9 shows the diffuse and wind field of PM_{10} of construction dust mean month in Xiamen in 2019.

It can be seen that there are differences in monthly dominant wind direction and wind speed in different regions, which eventually lead to seasonal differences in monthly average concentration distribution. Among them, the overall diffusion range of construction dust PM_{10} in Xiamen City in January 2019 moved from north to southwest, showing a zonal distribution; in April, the comprehensive diffusion range of construction dust PM_{10} moved from northeast to west in a zonal distribution; the overall diffusion range of construction dust PM_{10} in November showed a trend of continuous diffusion and aggregation to the southwest. Monthly average concentrations were lowest in July and highest in April.

Figure 10 shows the diffusion range of PM_{10} concentration gradient of construction dust in different representative months. It can be seen that the diffusion range of construction dust PM_{10} in Xiamen City in April 2019 was the largest, reaching 1657 km^2 . The diffusion range of

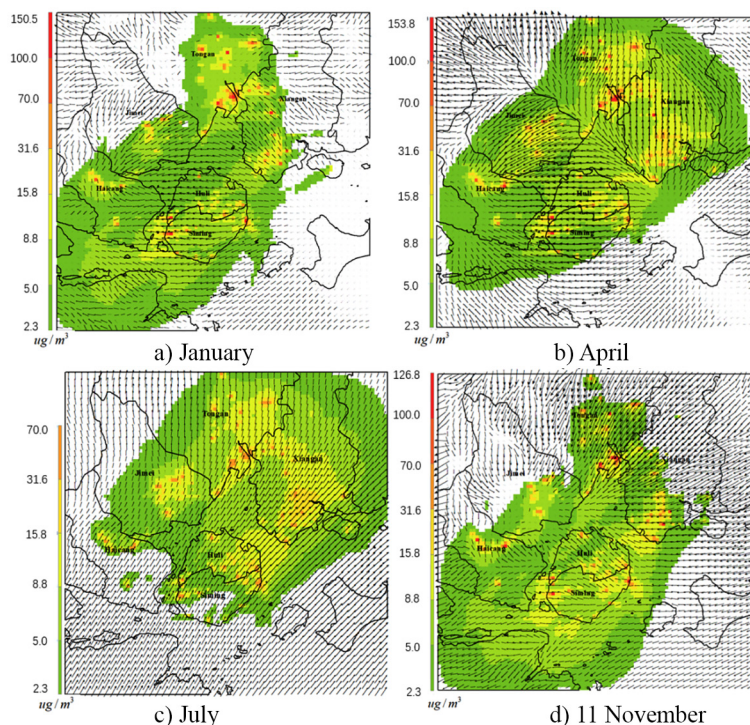


Figure 9. Monthly average PM_{10} concentration diffusion cloud map and wind field map of different representative month

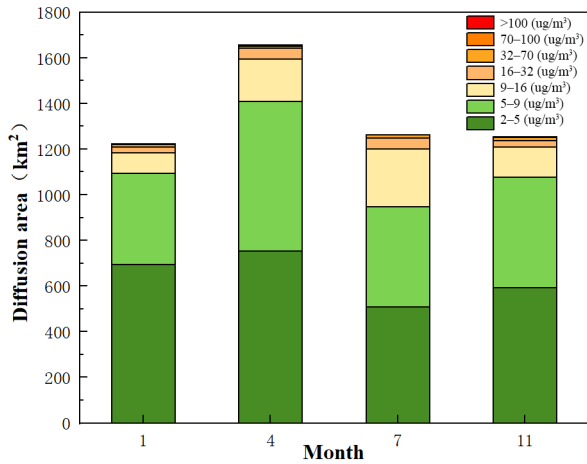


Figure 10. Diffusion range of monthly average concentration gradient of construction dust PM₁₀ under different representative months

construction dust PM₁₀ in the other three representative months had little change, maintaining at about 1200 km². The diffusion range of PM₁₀ monthly average concentration above 32 ug/m³ had little change, maintaining at about 15 km².

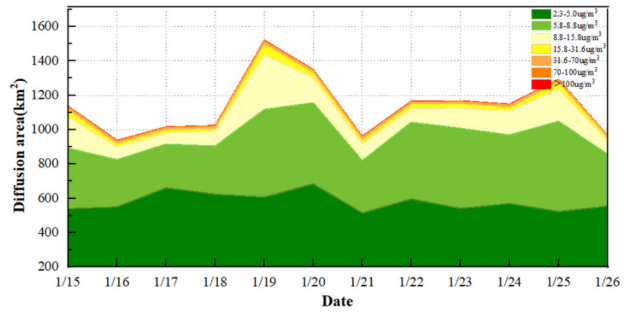


Figure 11. Time series variation chart of daily average concentration gradient diffusion range of construction dust PM₁₀

2.5. Analysis of simulation diffusion results of daily average concentration

To explore the influence of construction dust on the daily average concentration of PM₁₀, the simulated diffusion concentration results of construction dust PM₁₀ from January 15 to January 26 were extracted. Figure 11 shows the diffusion range of the daily average concentration gradient of construction dust PM₁₀. Figure 12 shows the diffusion map of daily average concentration and daily wind field map.

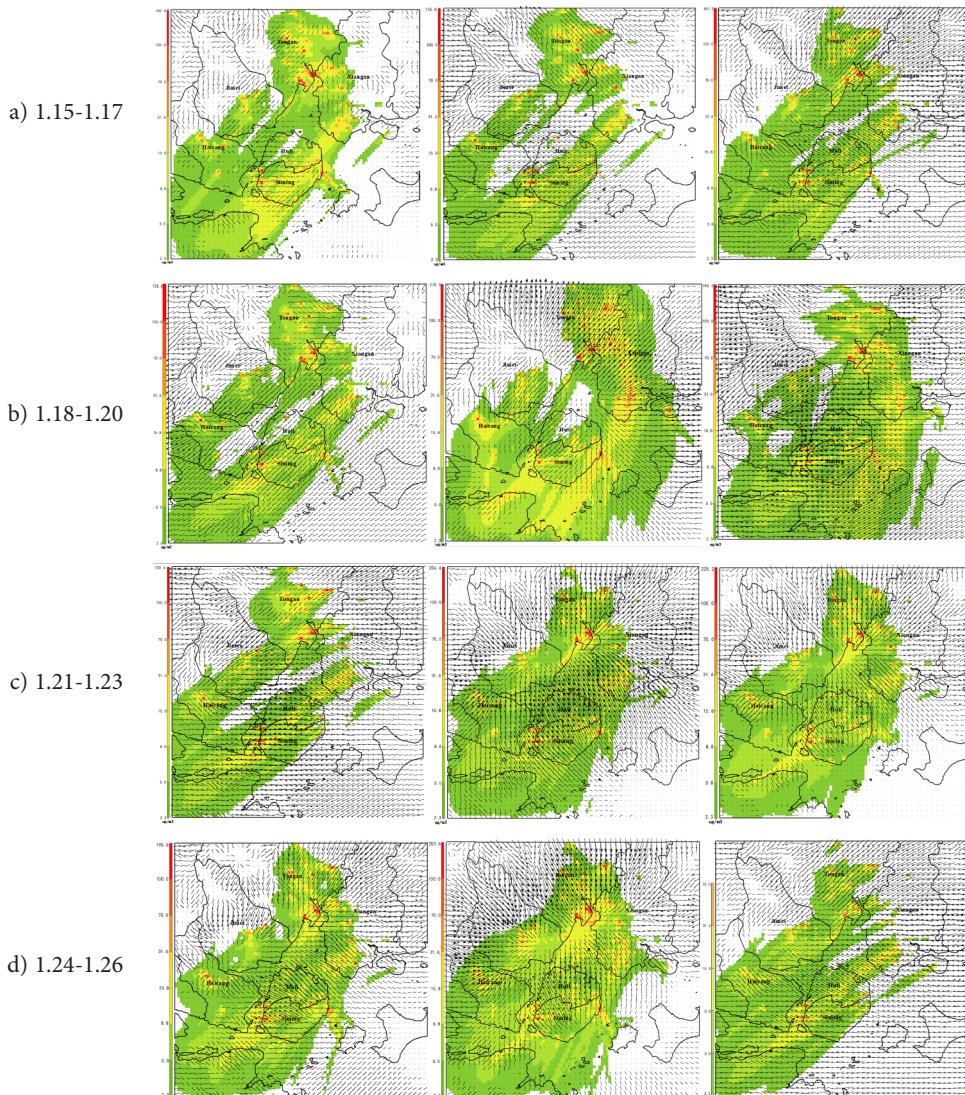


Figure 12. The daily average concentration diffusion map and daily average wind field map of construction dust PM₁₀ (1.15~1-26)

The above figures show that the diffusion area with PM₁₀ daily average concentration of less than 31.6 ug/m³ fluctuated during this period. The first trough appeared on January 16. The reasons for the analysis are as follows. On January 16, the dominant wind directions in Xiamen were east wind and southeast wind, with a single wind direction. In addition, the wind speed was much higher than that of the previous day, and the construction dust PM₁₀ rapidly dissipated in the same direction under the action of the wind. Then the first peak appeared on January 19. On that day, the wind direction of Xiamen City was radial as a whole. The daily dominant wind directions of each region were quite different, and the diffusion directions of dust in each region were inconsistent, which eventually led to the peak of the PM₁₀ diffusion range of construction dust. Subsequently, due to the change in wind direction, the daily dominant wind direction in all districts of Xiamen City turned to the east wind, which was blocked by buildings and terrain in one direction. The dissipation and settlement of PM₁₀ in construction dust accelerated and fell to the lowest value on January 21. After that, the wind direction inside the center island turned southward, the dominant wind direction in Haicang District and Jimei District turned southwestward, and the dominant wind direction in Tong'an District and Xiang'an District was northeastward. Multiple wind directions in opposite directions converge, enhancing the atmosphere's turbulence intensity and intensifying the turbulence movement. As a result, the construction dust PM₁₀ cannot quickly settle down, eventually leading to the increase in the daily average concentration of construction dust PM₁₀ and the expansion of the diffusion range.

It can be seen that wind direction and wind speed both were the main factors affecting the diffusion range and daily concentration gradient distribution of construction dust PM₁₀. When the dominant wind direction of the city was consistent, the greater the wind speed, blocked by one direction of terrain and buildings, the faster the construction dust PM₁₀ dissipated and settled in the same direction. The smaller the diffusion range of construction dust PM₁₀ was, the lower the daily average concentration of construction dust PM₁₀ would be. When the dominant wind direction of the city was inconsistent, the diffusion of PM₁₀ in construction dust would be intensified in two cases. The first was that the wind direction of the city was radial, which directly caused the radial diffusion of PM₁₀ in construction dust. The second was that the wind direction in all regions of the city was convergent, resulting in an increase in atmospheric turbulence intensity, which made the construction dust PM₁₀ unable to settle and dissipate, thereby indirectly causing an increase in the concentration and diffusion range of construction dust PM₁₀.

2.6. Analysis of the accuracy and credibility simulation diffusion results through hourly simulation on a certain day

Based on the results and analysis, it is known that the highest daily average concentration of PM₁₀ in Xiamen

occurred on January 20, 2019. The WRF model was mainly used to provide high-altitude meteorological simulation data for the CALMET module. To further verify the credibility of the results, this study investigated the diffusion pattern of construction dust within the urban area on that day. The period from 15:00 to 21:00 Beijing time on January 20, 2019 was selected as the study period, with the first three hours (15:00 to 18:00) as the continuous construction period and the last three hours (18:00 to 21:00) as the stop-work period. Meteorological data below 1 km from the ground level were analyzed, with a total of 38 layers in the vertical direction and a model maximum pressure of 50 hPa.

To test the accuracy and credibility of the WRF meteorological model simulation results at the mesoscale level, this study used the method of comparing simulated values with monitoring values. The monitoring values were hourly wind speed (10 m height) and wind direction angle (10 m height) data provided by the Xiamen ground meteorological station (station number 59134, longitude 118.07 degrees, latitude 24.48 degrees) from the China Meteorological Administration (CMA). The simulated values were hourly wind direction and speed data at the same location as the ground meteorological station in the WRF grid, covering 31 hours from January 20, 2019 02:00 to January 21, 2019 08:00 Beijing time. To evaluate the credibility of meteorological data, three indicators, bias (BIAS), mean absolute error (MAE), and root mean square error (RMSE), are generally used for quantitative evaluation. All three indicators are statistical quantities with dimensions, and the smaller the indicator value, the better the simulation effect. The specific calculation formulas are shown below (Lee et al., 2014; Li, 2017; Liu, 2012).

$$Bias = |M_{SIMULATEDi} - O_{MONITOREDi}|; \tag{12}$$

$$E = \frac{1}{N} \sum_{i=1}^N |M_{SIMULATEDi} - O_{MONITOREDi}|; \tag{13}$$

$$RMSE = \sqrt{\frac{\sum_{i=1}^N (M_{SIMULATEDi} - O_{MONITOREDi})^2}{N}}. \tag{14}$$

Table 5. WRF simulation value and monitoring value comparison results

Statistical index	Wind speed, m/s	Wind direction,°
<i>Bias</i> _{min}	0.087162	1.51
<i>Bias</i> _{max}	2.888432	333.18
<i>E</i>	1.236826	38.989
<i>RMSE</i>	1.513467	72.89

Figure 13 and Table 5 show that the root mean square error (RMSE) of wind speed is 1.236826 m/s, with a maximum deviation of 2.884329 m/s and a minimum deviation of 0.08893 m/s. The wind speed simulated by the WRF model during the early morning

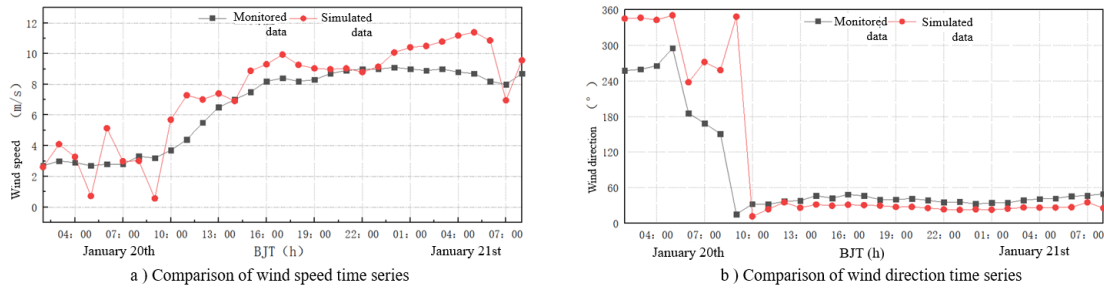


Figure 13. WRF simulation value and monitoring value time series comparison chart

to morning period (from 02:00 to 09:00 on January 20 and from 00:00 to 08:00 on January 21) shows a significant deviation from the monitoring values. The trend of wind speed variation simulated by WRF during the remaining time period is similar to the monitoring values, but the overall wind speed is still higher than the monitoring values. The results are in line with the reasonable error range given by previous scholars (Chang & Hanna, 2004; Lee et al., 2014; Yang et al., 2023). The discrepancy may be attributed to the fact that the monitoring values represent instantaneous values recorded once per hour at the meteorological station, while the simulated values represent hourly average values. Additionally, the simulation of wind speed during the transition period between day and night is affected by solar radiation. For the wind direction angle, the RMSE is 72.89 degrees, with a maximum deviation of 333.18 degrees and a minimum deviation of 1.51 degrees. The error in wind direction simulation by WRF mainly arises from the first eight hours of simulation. The trend and magnitude of wind direction angle simulated by WRF and monitored values are consistent during the 23 hours after 10:00 on January 20, 2019. The deviation in the first eight hours of simulation may be due to the resolution of the grid and terrain, as well as local turbulence fluctuations causing wind field abrupt changes. The results are in line with the previous scholars (Liu, 2012; Shi et al., 2022).

2.7. Regional contribution analysis of concentration simulation results of construction dust

To study the contribution relationship of construction dust PM₁₀ concentration between the six districts of Xiamen City and quantify the contribution ratio of construction dust concentration between different districts in different seasons representative months and throughout the year, several attention points were selected from each district of Xiamen City and the monthly average concentration of PM₁₀ at each attention point of the construction site in different districts in different representative months and the annual average concentration of PM₁₀ under the construction throughout the year were determined by the zero-return method. Then, the contribution relationship of construction dust PM₁₀ concentration between different districts in Xiamen in different seasons and the contribution relationship of construction dust PM₁₀ concentration in the whole year were indirectly determined.

Based on the population density and ventilation conditions, this paper selected two specific focus points in each area: one was in the urban building-intensive area, while another was located in open areas such as park suburbs. The specific location of the focus is shown in Figure 14.

Figure 15 shows the monthly average concentration contribution of construction dust PM₁₀ in representative months of different seasons and the annual average concentration contribution of construction dust PM₁₀.

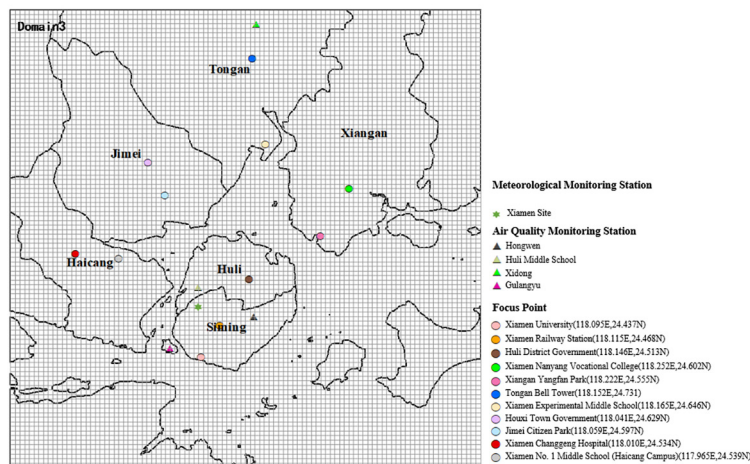


Figure 14. Positions of focus points and monitoring points

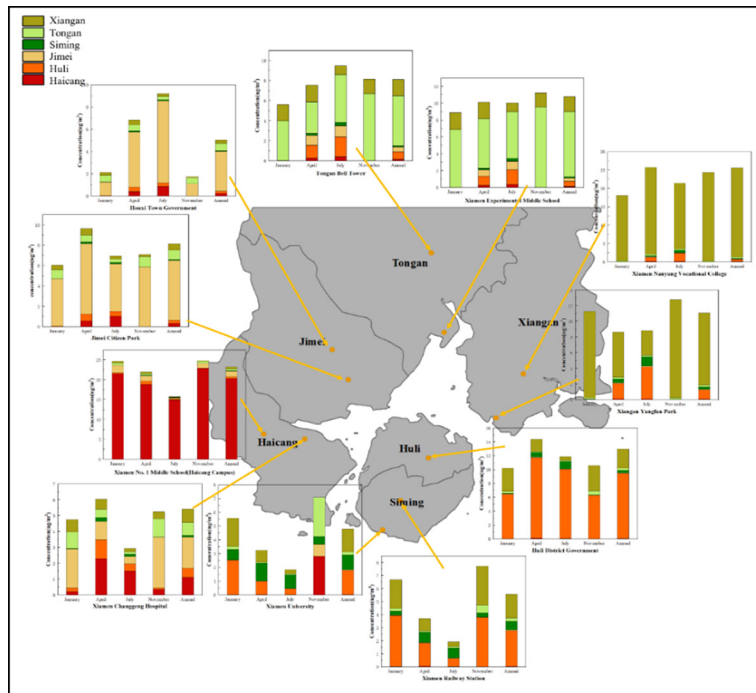


Figure 15. Statistics of contribution relationship of dust PM₁₀ concentration in construction on focus points

The monthly average concentration contribution sources of construction dust PM₁₀ under different representative months (except November) of the two focus points in Siming District were consistent with the annual average concentration contribution sources of construction dust PM₁₀. The main contribution sources were Xiang'an District, Huli District and Siming District from big to small. The monthly average PM₁₀ concentration of construction dust in Xiamen University in November was mainly contributed by Jimei District (11.3%), Haicang District (36.8%) and Tong'an District (37.7%), while the monthly average PM₁₀ concentration of construction dust in Xiamen Railway Station in November was mainly contributed by Tong'an District (7.7%), Xiang'an District (38.6%) and Huli District (48.9%).

The main sources of PM₁₀ annual average concentration contribution of construction dust in Huli District of the focus point (the government of Huli District) were Huli District (72.3%) and Xiang'an District (24.8%). The main sources of PM₁₀ monthly average concentration under different representative months (except July) were Huli District (59.3–80.6%) and Xiang'an District (12.3–34.7%). The monthly average PM₁₀ concentration contribution of construction dust in July by the local government was mainly from Huli District (83.9%) and Siming District (9.0%).

The contribution sources of PM₁₀ average annual concentration of construction dust of the two focus points in Xiang'an District were mainly Xiang'an District and Huli District. The monthly average PM₁₀ concentrations of construction dust in January and November of the two concerns were primarily contributed by the lake area (over 98%). The monthly average concentration contribution of

construction dust PM₁₀ in April and July of the two focus points mainly came from Huli District and Xiang'an District.

The annual average concentration contribution of construction dust PM₁₀ of the two focus points in Tong'an District mainly came from Tong'an District, Xiang'an District and Huli District. The contribution of PM₁₀ monthly average concentration of construction dust in January and November mainly came from Tong'an District (70.2–85.0%) and Xiang'an District (15.0–29.2%). The monthly average PM₁₀ concentration contribution of construction dust in April and July was mainly from Tong'an District (41.5–58.0%), Huli District (10.5–20.8%), Xiang'an District (9.3–22.0%) and Jimei District (7.7–12.9%).

The annual average PM₁₀ concentration of construction dust of the two focus points in Jimei District was contributed by four areas: Jimei District (70–72%), Tong'an District (11.5–12.4%), Xiang'an District (7.0–7.5%) and Haicang District (3.9–4.7%). The contribution of PM₁₀ monthly average concentration of construction dust in January and November mainly came from Jimei District (56.7–82.5%), Tong'an District (13.9–32.0%), and Xiang'an District (3.3–12.2%). The monthly average PM₁₀ concentration contribution of construction dust in April and July of the two concerns was mainly from Jimei District (71.3–72.2%), Tong'an District (7–7.7%), Xiang'an District (6.7%), Huli District (6.0–7.0%) and Haicang District (5.7–6.0%).

The average annual concentration contribution and monthly concentration contribution sources of construction dust PM₁₀ of the two focus points (Campus of Xiamen No. 1 Middle School and Xiamen Changgeng Hospital) in Haicang were quite different. The annual average

concentration contribution and monthly average concentration contribution of construction dust PM₁₀ in Haicang Campus of Xiamen No.1 Middle School were mainly from the local Haicang District, followed by Jimei District. Due to the special terrain, the dominant wind direction in this area formed a rotating wind, and the local source cannot diffuse outward, resulting in a large proportion of local sources. For Xiamen Changgeng Hospital, the average annual concentration contribution and monthly concentration contribution of construction dust PM₁₀ were mainly from Jimei District, Haicang District, Xiang'an District, Tong'an District, and Huli District, and the contribution proportion showed seasonal changes.

Conclusions

This paper simulated the diffusion of construction dust in the urban area of Xiamen with the tools of WRF and CALPUFF in case of all construction sites were working at the same time. The main conclusions are as follows:

- 1) If all the construction sites are under construction, the overall diffusion range of dust PM₁₀ in Xiamen City in 2019 will be zonally distributed from northeast to southwest. In the monthly average concentration gradient distribution of construction dust PM₁₀, the seasonal difference is mainly reflected in the area where the monthly average concentration of construction dust PM₁₀ is below 32 ug/m³.
- 2) Assuming that the construction sites in the six districts of Xiamen are opened separately, the diffusion conditions in Xiang'an District are the best, and the diffusion range of PM₁₀ is the largest. The construction dust PM₁₀ is not easy to diffuse, and the diffusion range of construction dust PM₁₀ is the smallest in Haicang District. In the construction dust PM₁₀ regional concentration contribution, some areas show prominent seasonal characteristics.
- 3) The best start time of Siming district and Haicang District is the end of the year or the beginning of the year; Summer is the best time to start construction of sites in Huli District; Construction sites in Xiang'an District and Tong'an District should be arranged between spring and summer; the optimal starting time for the site in Jimei District is January.

Although the WRF and CALPUFF model were combined to simulate the diffusion distribution of long-distance pollutants over 50 km of construction dust PM₁₀ monitoring index in this paper, the research on the diffusion distribution of construction dust at the urban level is still a huge systematic problem remaining to be focused on. For example, observation and measurements have been compared, assuming a constant 27% contribution of construction to measured concentrations everywhere in the town. This is not very quantitative. The next research step can try to create a method to obtain the PM₁₀ generated only by the construction dust diffusion and simulate the larger scale diffusion based on it. Furthermore, the

emission disperses in the urban area near ground level, so buildings and urban obstacles influence the transport and dispersion. These effects were not taken into account in the paper. How to consider urban construction to study the law of construction dust diffusion is a worthwhile and challenging future research direction.

Acknowledgements

This research is supported by the National Natural Science Foundation of China (Grant No. 71871192), "Xiamen City Construction Technology Project 2020" (XJK2020-1-6), China Railway South Investment Group Co., Ltd., the 2016 major scientific and technological plan "Xiamen Metro Line 3 across the sea tunnel construction risk control and system development".

References

- Akhmetshina, A. S., Kizhner, L. I., Kuzhevskaya, I. V., Bart, A. A., Zuev, V. V., & Shelekhov, A. P. (2015, June 22–26). Using WRF mesoscale model to restore temperature profile in atmosphere boundary layer in Tomsk. *Proceedings of SPIE*, 9680. <https://doi.org/10.1117/12.2205590>
- Bo, X., Ding, F., Xu, H., & Li, S. (2009). Review of atmospheric diffusion CALPUFF model technology. *The Administration and Technique of Environmental Monitoring*, 21(03), 9–13+47. https://kns.cnki.net/kcms/detail/detail.aspx?dbcode=CJFD&dbname=CJFD2009&filename=HJJS200903006&uniplatform=NZKPT&v=B-udfVJQslXSwbUP44yQXjp9lkTMZ5D2x_S0-rJNGAqpc_QGeQ7TbLnwVWRLIPf3
- Chang, J. C., & Hanna, S. R. (2004). Air quality model performance evaluation. *Meteorology and Atmospheric Physics*, 87(1–3), 167–196. <https://doi.org/10.1007/s00703-003-0070-7>
- Chen, S. Y., Zhang, X. R., Lin, J. T., Huang, J. P., Zhao, D., Yuan, T. G., Huang, K. N., Luo, Y., Jia, Z., Zang, Z., Qiu, Y. A., & Xie, L. (2019). Fugitive road dust PM_{2.5} emissions and their potential health impacts. *Environmental Science & Technology*, 53(14), 8455–8465. <https://doi.org/10.1021/acs.est.9b00666>
- Choi, G.-S., Lim, J.-M., Lim, K.-S. S., Kim, K.-H., & Lee, J.-H. (2018). Characteristics of regional scale atmospheric dispersion around Ki-Jang research reactor using the Lagrangian Gaussian puff dispersion model. *Nuclear Engineering and Technology*, 50(1), 68–79. <https://doi.org/10.1016/j.net.2017.10.002>
- Cui, H., Yao, R., Xu, X., Xin, C., & Yang, J. (2011). A tracer experiment study to evaluate the CALPUFF real time application in a near-field complex terrain setting. *Atmospheric Environment*, 45(39), 7525–7532. <https://doi.org/10.1016/j.atmosenv.2011.08.041>
- Cui, M., Wang, X., Su, H., & Zhang, Y. (2008). Chemical characteristics and source analysis of atmospheric inhalable particles in Guangzhou. *Acta Scientiarum Naturalium Universitatis Pekinensis*, (03), 459–466. <https://doi.org/10.13209/j.0479-8023.2008.072>
- Fan, W., Chen, J., Tang, B., Feng, X., & Luo, L. (2022). Study on emission inventory of building construction dust in Guangyuan City. *Sichuan Environment*, 41(01), 113–118. <https://doi.org/10.14034/j.cnki.schj.2022.01.018>
- Fan, W., Chen, J., Tang, B., Feng, X., Sun, H., Zhang, Y., Wang, J., Jing, C., Luo, L., Jiang, T., Wu, K., Sun, S., Jiang, T., Qian, J., & Liu, Z. (2020). Study on dust emission characteristics of con-

- struction in Chengdu. *China Environmental Science*, 40(09), 3767–3775.
<https://doi.org/10.19674/j.cnki.issn1000-6923.2020.0421>
- Fisher, A. L., Parsons, M. C., Roberts, S. E., Shea, P. J., Khan, F. I., & Husain, T. (2003). Long-term SO₂ dispersion modeling over a coastal region. *Environmental Technology*, 24(4), 399–409. <https://doi.org/10.1080/09593330309385574>
- Gehrig, R., & Buchmann, B. (2003). Characterising seasonal variations and spatial distribution of ambient PM₁₀ and PM_{2.5} concentrations based on long-term Swiss monitoring data. *Atmospheric Environment*, 37(19), 2571–2580.
[https://doi.org/10.1016/s1352-2310\(03\)00221-8](https://doi.org/10.1016/s1352-2310(03)00221-8)
- Guo, D. P., Wang, R., & Zhao, P. (2020). Spatial distribution and source contributions of PM_{2.5} concentrations in Jincheng, China. *Atmospheric Pollution Research*, 11(8), 1281–1289.
<https://doi.org/10.1016/j.apr.2020.05.004>
- Holnicki, P., Kaluszko, A., & Trapp, W. (2016). An urban scale application and validation of the CALPUFF model. *Atmospheric Pollution Research*, 7(3), 393–402.
<https://doi.org/10.1016/j.apr.2015.10.016>
- Huang, Y., Cai, Y., Mao, H., Sheng, L., Qin, J., & Yan, J. (2011). Emission factors and particle size distribution of construction dust in Hohhot. *Journal of Inner Mongolia University (Natural Science Edition)*, 42(02), 230–235. <https://kns.cnki.net/kcms/detail/detail.aspx?dbcode=CJFD&dbname=CJFD2011&filename=NMGX201102019&uniplatform=NZKPT&v=uYab8mdtNEO7xXl6mD8lrP2KiogtFOYrwA7DOeDfiqRyRUO17QLhnXdgaCX0P7ml>
- Lee, H. D., Yoo, J. W., Kang, M. K., Kang, J. S., Jung, J. H., & Oh, K. J. (2014). Evaluation of concentrations and source contribution of PM₁₀ and SO₂ emitted from industrial complexes in Ulsan, Korea: Interfacing of the WRF-CALPUFF modeling tools. *Atmospheric Pollution Research*, 5(4), 664–676.
<https://doi.org/10.5094/apr.2014.076>
- Lei, T., Li, B., Bo, X., Qu, J., Ma, Y., Mao, N., & Lu, R. (2021). Evaluation of emission reduction of cangzhou foundry industry based on CALPUFF. *Environmental Impact Assessment*, 43(05), 68–74. <https://doi.org/10.14068/j.ceia.2021.05.015>
- Li, B. (2014). *Research on methods of improving atmospheric environmental impact prediction level in coking industry* [Master's thesis, Lanzhou University]. <https://kns.cnki.net/KCMS/detail/detail.aspx?dbname=CMFD201402&filename=1014301835.nh>
- Li, H. (2017). *A study on the inflow turbulence in simulation of microscale atmospheric environment by multi-scale coupling method* [Doctoral dissertation, Tsinghua University]. China.
- Li, M., Yang, D., & He, W. (2020). Comparison and perspectives on theories and simulation results of gas dispersion models AERMOD and CALPUFF. *Geomatics and Information Science of Wuhan University*, 45(08), 1245–1254.
<https://doi.org/10.13203/j.whugis20200110>
- Li, Y., & Guo, H. (2006). Comparison of odor dispersion predictions between CFD and CALPUFF models. *Transactions of the Asabe*, 49(6), 1915–1926. <https://doi.org/10.13031/2013.22293>
- Lim, K.-S. S., Lim, J.-M., Lee, J., & Shin, H. H. (2021). Impact of boundary layer simulation on predicting radioactive pollutant dispersion: A case study for HANARO research reactor using the WRF-MMIF-CALPUFF modeling system. *Nuclear Engineering and Technology*, 53(1), 244–252.
<https://doi.org/10.1016/j.net.2020.06.011>
- Liu, X. (2015). *Simulation of PM_{2.5} regional transmission in Beijing-Tianjin-Hebei Region* [Doctoral dissertation, Tsinghua University]. https://kns.cnki.net/kcms/detail/detail.aspx?dbcode=CDFD&dbname=CDFDLAST2016&filename=1016712159.nh&uniplatform=NZKPT&v=-v-iifNI1-AUKGC2_I-cELvYv8sD-Jcc33RrQJ3NDBK5o8WLW01M3P-5nrr1BJ8Uz
- Liu, Y. (2012). *Large eddy simulation of urban micro-atmospheric environment* [Doctoral dissertation, Tsinghua University]. China.
- Ministry of Ecology and Environment of the Peoples Republic of China. (2018). *Technical guidelines for environmental impact assessment-atmospheric environment* (HJ 2.2-2018). Standards Press of China. https://www.mee.gov.cn/ywgz/fgbz/bz/bzwb/other/pjjsdz/201808/t20180814_451386.shtml
- Ministry of Ecology and Environment the People's Republic of China. (2014). *Technical guide for the preparation of dust source particulate emission inventory (Trial)*. https://www.mee.gov.cn/gkml/hbb/bgg/201501/t20150107_293955.htm
- Peckham, S. E. (2012). *WRF/Chem version 3.3 user's guide*. <https://repository.library.noaa.gov/view/noaa/11119>
- Rui, D., Chen, J., & Feng, Y. (2008). Source apportionment of PM₁₀ in Nanjing. *Environmental Science and Management*, (04), 56–58+61. <https://kns.cnki.net/kcms/detail/detail.aspx?dbcode=CJFD&dbname=CJFD2008&filename=BFHJ200804015&uniplatform=NZKPT&v=j6Uat3naGufkjV79BT7aSaGY379lKkimiMEflQBMk6eeJeZSrzchxA7pb0Yi4j>
- Shi, X., Guo, D. P., Wang, R., Li, Y., & Yao, R. (2022). Effects on pollutant dispersion over complex terrain on CALPUFF model. *Radiation Protection*, 42(05), 433–441.
- Skamarock, W. C., Klemp, J. B., Dudhia, J., Gill, D. O., Barker, D., Duda, M. G., Huang, X.-y., Wang, W., & Powers, J. G. (2008). *A description of the advanced research WRF version 3* (No. NCAR/TN-475+STR). University Corporation for Atmospheric Research. <https://doi.org/10.5065/D68S4MVH>
- Song, B., Huang, Y., Qin, J., Li, B., Zhang, C., & Shi, A. (2019). Overview of test methods for dust emission factors of construction in China and abroad. *Environmental Engineering*, 37(04), 126–130. <https://doi.org/10.13205/j.hjgc.201904024>
- Sówka, I., Kobus, D., Skotak, K., Zathay, M., Merenda, B., & Paciorek, M. (2019). Assessment of the health risk related to air pollution in selected polish health resorts. *Journal of Ecological Engineering*, 20(10), 132–145.
<https://doi.org/10.12911/22998993/113142>
- Statistics, X. M. B. o. (2020, March 20). *National Economic and Social Development Statistics Bulletin of Xiamen in 2019*. A06. <https://doi.org/10.28890/n.cnki.nxmrb.2020.001228>
- Tartakovsky, D., Stern, E., & Broday, D. M. (2016). Dispersion of TSP and PM₁₀ emissions from quarries in complex terrain. *Science of the Total Environment*, 542, 946–954.
<https://doi.org/10.1016/j.scitotenv.2015.10.133>
- Todd, M. C., & Cavazos-Guerra, C. (2016). Dust aerosol emission over the Sahara during summertime from Cloud-Aerosol Lidar with Orthogonal Polarization (CALIOP) observations. *Atmospheric Environment*, 128, 147–157.
<https://doi.org/10.1016/j.atmosenv.2015.12.037>
- United States Environmental Protection Agency. (1995). *AP-42: Compilation of air pollutant emission factors* (5th ed.). Research Triangle Park.
- Venkatram, A. (2004). On estimating emissions through horizontal fluxes (vol 38, pg 1337, 2004). *Atmospheric Environment*, 38(14), 2209. <https://doi.org/10.1016/j.atmosenv.2004.02.012>
- Veranth, J. M., Pardyjak, E. R., & Seshadri, G. (2003). Vehicle-generated fugitive dust transport: Analytic models and field study. *Atmospheric Environment*, 37(16), 2295–2303.
[https://doi.org/10.1016/s1352-2310\(03\)00086-4](https://doi.org/10.1016/s1352-2310(03)00086-4)
- Wu, P. (2018). *Study on health effects of major air pollutants in Linyi city* [Master's thesis, Capital University of Economics and

- Business]. https://kns.cnki.net/kcms/detail/detail.aspx?dbcode=CMFD&dbname=CMFD201901&filename=1018141620.nh&uniplatform=NZKPT&v=EcfjX_AD27gj0Gw1LhdOR6q6CGSK5An8lh7llV8kL7cb5H4u_tbUAHVZy4ps7kID
- Xiao, S., Cai, M., Li, X., Huang, Z., Wang, J., Zhu, Q., & Wu, S. (2022). Characterization and health risk assessment of heavy metals in PM_{2.5} in Xiamen Port. *Environmental Science*, 43(07), 3404–3415. <https://doi.org/10.13227/j.hjcx.202110163>
- Xing, J. D., Ye, K. H., Zuo, J., & Jiang, W. Y. (2018). Control dust pollution on construction sites: What governments do in China? *Sustainability*, 10(8), 2945. <https://doi.org/10.3390/su10082945>
- Xu, H., Zhu, Y., Wang, L., Lin, C. J., Jang, C., Zhou, Q., Yu, B., Wang, S. X., Xing, J., & Yu, L. (2019). Source contribution analysis of mercury deposition using an enhanced CALPUFF-Hg in the central Pearl River Delta, China. *Environmental Pollution*, 250, 1032–1043. <https://doi.org/10.1016/j.envpol.2019.04.008>
- Xu, Q., Zhou, G., Duan, H., Li, X., Yin, W., & Tang, Y. (2022). *Accounting of fugitive emissions in steel plant with aeromod model* [Conference presentation]. 2022 Annual Conference of Science and Technology of Chinese Society of Environmental Sciences – Branch of Environmental Engineering Technology Innovation and Application, Nanchang, Jiangxi, China.
- Yan, H., Ding, G. L., Li, H. Y., Wang, Y. S., Zhang, L., Shen, Q. P., & Feng, K. L. (2019). Field evaluation of the dust impacts from construction sites on surrounding areas: A city case study in China. *Sustainability*, 11(7), 1906. <https://doi.org/10.3390/su11071906>
- Yang, J., Jiang, X., Bo, X., Wang, G., & Feng, Y. (2023). Large eddy simulation of urban micro-atmospheric environment. *Environmental Science*, 44(01), 104–117.
- Yang, T., He, Y., Liu, Y., Sun, L., & Wang, H. (2022). *Simulation of dust pollution diffusion in urban construction sites* [Conference presentation]. 2022 Annual Conference of Science and Technology, Chinese Society of Environmental Sciences, Nanchang, Jiangxi, China.
- Yang, Y. (2014). *Character, level and regulatory measures study of fugitive dust emissions from building construction sites in PRD* [Master's thesis, South China University of Technology]. China.
- Yang, Y., Zhao, Y., Zhang, L., & Lu, Y. (2019). Evaluating the methods and influencing factors of satellite-derived estimates of NO_x emissions at regional scale: A case study for Yangtze River Delta, China. *Atmospheric Environment*, 219, 117051. <https://doi.org/10.1016/j.atmosenv.2019.117051>
- Zhang, L., Li, L., Jiang, L., Zhao, W., Lu, H., Wang, X., & Qiu, Y. (2019). Spatio-temporal variation of bare land in Beijing construction and dust emission. *Environmental Science*, 40(01), 135–142. <https://doi.org/10.13227/j.hjcx.201804236>
- Zhang, R., Li, M., Yang, D., & Liu, H. (2022). Three dimensional dynamic simulation method of toxic gas leakage accident based on CALPUFF model: A case study of Gaoqiao Town. *Acta Scientiarum Naturalium Universitatis Pekinensis*, 1–15.
- Zhang, Y., Liu, P., Pun, B., & Seigneur, C. (2006). A comprehensive performance evaluation of MM5-CMAQ for the Summer 1999 Southern Oxidants Study episode – Part I: Evaluation protocols, databases, and meteorological predictions. *Atmospheric Environment*, 40(26), 4825–4838. <https://doi.org/10.1016/j.atmosenv.2005.12.043>
- Zhang, Y., Sartelet, K., Wu, S. Y., & Seigneur, C. (2013a). Application of WRF/Chem-MADRID and WRF/Polyphemus in Europe – Part I: Model description, evaluation of meteorological predictions, and aerosol-meteorology interactions. *Atmospheric Chemistry and Physics*, 13(14), 6807–6843. <https://doi.org/10.5194/acp-13-6807-2013>
- Zhang, Y., Sartelet, K., Zhu, S., Wang, W., Wu, S.-Y., Zhang, X., Wang, K., Tran, P., Seigneur, C., & Wang, Z.-F. (2013b). Application of WRF/Chem-MADRID and WRF/Polyphemus in Europe – Part 2: Evaluation of chemical concentrations and sensitivity simulations. *Atmospheric Chemistry and Physics*, 13(14), 6845–6875. <https://doi.org/10.5194/acp-13-6845-2013>
- Zhao, D., & Li, X. (2018). Comparative study of atmospheric diffusion model AERMOD and CALPUFF. In *2018 Annual Meeting of Science and Technology of Chinese Society of Environmental Sciences*, Hefei, Anhui, China.
- Zhao, L. (2020). *Transfer characteristics and source apportionment of heavy metals in the dust-soil-plant system at the park sites in Xiamen* [Doctoral dissertation, Huaqiao University]. China. <https://doi.org/10.27155/d.cnki.gHQIU.2020.000702>
- Zhao, W., Fan, S., & Xie, W. (2015). A comparison of AERMOD with CALPUFF for coastal power plant flue gas dispersion modeling. *Environmental Science and Technology*, 38(03), 189–194. <https://doi.org/10.3969/j.issn.1003-6504.2015.03.035>
- Zhou, H., Shen, X., & Zhao, Y. (2022). Research on simulation of construction dust diffusion and quantitative assessment for damage on workers' health. *Journal of Safety and Environment*, 1–10.
- Zhu, K. (2020). *Spatial and temporal pattern of dust in changsha urban area and analysis of influencing factors* [Master's thesis, Hunan Normal University]. China. <https://doi.org/10.27137/d.cnki.gHUSU.2020.002000>